

# HII-CHI-mistry: A collection of python scripts for the analysis of emission lines in ionized gaseous nebulae

Enrique Pérez-Montero

Instituto de Astrofísica de Andalucía - CSIC. Apdo. 3004, 15080, Granada, Spain

## 1. General description

### 1.1. *What is HII-CHI-MISTRY and where can it be found?*

Ionized gaseous nebulae are ubiquitous objects in the Universe that provide valuable information about the galaxies where they reside through their bright emission lines. Among the various properties that can be derived from these nebulae are the relative chemical abundances of observed ions, the excitation of the gas, and the effective hardening of the ionizing source.

HII-CHI-MISTRY (hereinafter, HCM) is a collection of Python scripts designed to analyze observational data from several bright emission lines observed in the ultraviolet, optical, or infrared ranges of the spectrum. By comparing these observations with predictions from extensive grids of photoionization models, HCM provides estimates and associated uncertainties for several derived properties, adapting the accuracy of the solutions based on the input lines and their uncertainties.

HCM offers three main advantages for the calculation of chemical abundances compared to other model-based solutions:

1. The results are entirely consistent with the direct method, which relies on the prior determination of the electron temperature. This holds true even when the flux of an auroral line, such as  $[[\text{O III}]] \lambda 4363 \text{ \AA}$ , is not used (see Pérez-Montero, 2014).
2. HCM provides consistent solutions regardless of the set of input emission lines and their errors. This is particularly useful when comparing results for different sets of objects observed with varying spectral ranges or redshifts.
3. HCM provides independent solutions for N/O (in the optical and infrared) or C/O (in the ultraviolet), allowing for the determination of O/H using N or C without assuming a relationship between O/H and N/O or C/O.

In this tutorial, I explain the features of the different versions of the code, their usage instructions, limitations, and expected future improvements. There are five versions of HCM depending on the spectral range and whether they are used for determining chemical abundances or calculating the hardening of the ionizing source. These versions are:

- HII-CHI-MISTRY: The original HCM package described in Pérez-Montero, 2014 for analyzing gaseous nebulae ionized by massive young star clusters, and in Pérez-Montero et al., 2019a for Narrow Line Regions (NLR) ionized by active galactic nuclei (AGN). It is used to derive the total oxygen abundance ( $12+\log(\text{O}/\text{H})$ , hereafter O/H), the nitrogen-to-oxygen chemical abundance ratio ( $\log(\text{N}/\text{O})$ , hereafter N/O), and the ionization parameter ( $\log U$ ) using optical emission lines from  $[[\text{O II}]] \lambda 3727 \text{ \AA}$  up to  $[[\text{S III}]] \lambda 9069,9532 \text{ \AA}$ .

- HII-CHI-MISTRY-UV: Described in Pérez-Montero and Amorín, 2017 for star-forming objects, and in Pérez-Montero et al., 2023a for the NLR of AGN. It calculates O/H, the carbon-to-oxygen chemical abundance ratio ( $\log(\text{C}/\text{O})$ , hereafter C/O), and  $\log U$ , using ultraviolet emission lines from  $\text{Ly}\alpha \lambda 1216 \text{ \AA}$  up to  $\text{C III}] \lambda 1909 \text{ \AA}$ .

- HII-CHI-MISTRY-IR: Described in Fernández-Ontiveros et al., 2021 for star-forming

objects, and in Pérez-Díaz et al., 2022 for the NLR of AGNs. It calculates O/H, N/O, and  $\log U$  using infrared emission lines from Br $\alpha$   $\lambda$  4.05  $\mu\text{m}$  up to [[N II]]  $\lambda$  205  $\mu\text{m}$ .

- HII-CHI-MISTRY-TEFF: It calculates the equivalent effective temperature ( $T_*$ ) and  $\log U$  using optical and UV emission lines and O/H, as described in Pérez-Montero et al., 2019b. It can also be used to derive the fraction of absorbed ionizing photons for objects with He II  $\lambda$  4686 Å, as described in Pérez-Montero et al., 2020.

- HCM-TEFF-IR: It calculates  $T_*$  and  $U$  based on near- and mid-infrared emission lines, as described in Pérez-Montero et al., 2024. It can also calculate the parameter  $\alpha_{OX}$ , indicative of the hardness of the incident SED of AGN taking advantage of the very high-excitation lines present in this regime (see Pérez-Montero, submitted)..

HCM has been originally written in python v. 2.7, but from version 5 is only compatible with python 3. It can be downloaded from the HCM webpage at <http://home.iaa.es/~epm/HII-CHI-mistry.html>. In this document, I describe features for the public versions of HCM 5.4 and equivalent versions, which require the Python library `numpy`. Each package contains the corresponding script (with a `.py` extension), an ASCII file with instructions, an example input text file, and different libraries containing model information and template files for constrained sub-grids used by the code in the absence of certain emission lines. All files are included in a compressed `tgz` file, which can be uncompressed using the following command in a terminal prompt:

```
> tar xvfz HCM.v5.4.tar.gz
```

### 1.2. How does the code work?

All versions of HCM employ a Bayesian-like approach to derive chemical abundances, the ionization parameter, or  $T_*$ . In brief, for a given property  $X$ , the final result is calculated as follows:

$$X_f = \frac{\sum_i X_i / \chi_i}{\sum_i 1 / \chi_i} \quad (1.1)$$

where  $X_f$  is the final result,  $X_i$  are the input values from each model in the grid, and  $\chi_i$  are the weights assigned to each model, calculated as the quadratic difference between the observed and predicted values for specific emission-line ratios:

$$\chi_i^2 = \sum_j \frac{(O_j - T_{ji})^2}{O_j} \quad (1.2)$$

where  $O_j$  and  $T_{ji}$  are the observed and model-based values, respectively, for the considered emission-line dependent ratios. These ratios are described in each of the papers on the different versions of HCM as a function of the input emission lines. Notice that, contrary to a pure bayesian method, in which the model with a least  $\chi^2$  is selected, this method provides a more realistic estimation of the derived properties, even if the nominal values are not given in the models, with their corresponding uncertainty.

The errors assigned to each result are calculated as the quadratic sum of the dispersion of all results obtained through a Monte Carlo iteration of the nominal values perturbed with the input observational errors, and the mean of all intrinsic uncertainties assigned to the Bayesian process, calculated as:

$$(\Delta X)^2 = \frac{\sum_i (X_f - X_i)^2 / \chi_i}{\sum_i 1 / \chi_i} \quad (1.3)$$

For the versions of HCM aimed at calculating chemical abundances, the first iteration provides an estimation for the abundance of a secondary ion (N for HCM and HCM-IR, or C for HCM-UV), relative to oxygen. These estimations are based on emission-line ratios that are not very sensitive to  $\log U$ . This allows the grid to be constrained in a second iteration, once N/O or C/O are fixed, to calculate both O/H and  $\log U$  using N or C lines without any a priori assumption about the relationship between O and the respective secondary element.

In the case of HCM-TEFF, both for optical and IR, this previous iteration is not performed. Instead, the grid of models is interpolated to fix the value of O/H to the input value in order to minimize the dependence of both  $T_*$  and  $U$  on metallicity.

## 2. HCM in the optical

### 2.1. Running the program

To run the HCM code version 5.4, type the following command in the terminal prompt:

```
> python HCM.v5.4.py
```

A description of the code will appear on the screen, and it will prompt for the input file containing the observational information. Alternatively, the input file name and the desired number of iterations for the Monte Carlo simulation can be specified when invoking the code:

```
> python HCM.v5.4.py input.txt 100
```

If the number of iterations is not specified, it defaults to 25.

### 2.2. The input file

The input file must be an ASCII file, with as many rows as the number of objects or pointings for which the calculations are to be performed. Each column represents the identification for each row and the reddening-corrected fluxes relative to  $H\beta$  with their corresponding errors. In previous versions of HCM, all columns needed to be introduced, but from version 5.0 onwards, a first row with the labels of the introduced columns is required, and the order is not essential. The file can also include other columns not identified by the code. The columns assigned to the observational relative errors are optional. The labels for the emission lines in this version are:

- ID: To identify each row with a name.
- OII\_3727 and eOII\_3727: For  $[[\text{O II}]] \lambda 3727 \text{ \AA}$  and its error. This is assumed to be the sum of  $\lambda 3726 \text{ \AA}$  and  $\lambda 3729 \text{ \AA}$  in resolved spectra.
- NeIII\_3868 and eNeIII\_3868: For  $[[\text{Ne III}]] \lambda 3868 \text{ \AA}$  and its error.
- OIII\_4363 and eOIII\_4363: For  $[[\text{O III}]] \lambda 4363 \text{ \AA}$  and its error.
- OIII\_4959 and eOIII\_4959: For  $[[\text{O III}]] \lambda 4959 \text{ \AA}$  and its error.
- OIII\_5007 and eOIII\_5007: For  $[[\text{O III}]] \lambda 5007 \text{ \AA}$  and its error. When only one of the two strong  $[[\text{O III}]]$  lines is provided, the code assumes the theoretical ratio between them.
- NII\_5755 and eNII\_5755: For  $[[\text{N II}]] \lambda 5755 \text{ \AA}$  and its error.

- SIII\_6312 and eSIII\_6312: For  $[[\text{S III}]] \lambda 6312 \text{ \AA}$  and its error.
- NII\_6584 and eNII\_6584: For  $[[\text{N II}]] \lambda 6584 \text{ \AA}$  and its error.
- SII\_6716 and eSII\_6716: For  $[[\text{S II}]] \lambda 6716 \text{ \AA}$  and its error.
- SII\_6731 and eSII\_6731: For  $[[\text{S II}]] \lambda 6731 \text{ \AA}$  and its error. Note that the code will only use the  $[[\text{S II}]]$  lines if both of them or their sum is provided.
- Alternatively, the sum of these two lines can be given as SII\_6725 and eSII\_6725.
- OII\_7325 and eOII\_7325: For  $[[\text{O II}]] \lambda\lambda 7319+7330 \text{ \AA}$  and its error.
- SIII\_9069 and eSIII\_9069: For  $[[\text{S III}]] \lambda 9069 \text{ \AA}$  and its error.
- SIII\_9532 and eSIII\_9532: For  $[[\text{S III}]] \lambda 9532 \text{ \AA}$  and its error. When only one of the two strong  $[[\text{S III}]]$  lines is provided, the code assumes the theoretical ratio between them.

### 2.3. Selecting the grid of models

If the input file is correct, the code will prompt you to select the grid of models to perform the calculation:

- (1) POPSTAR with Chabrier IMF, age = 1 Myr
- (2) BPASS v.2.1 a\_IMF = 1.35, Mup = 300, age = 1 Myr with binaries
- (3) AGN, double component,  $\alpha(\text{UV}) = -1.0$

Other SED

- (4) Different library

Choose SED of the models:

All grids have been calculated using the code CLOUDY v.17 (Ferland et al., 2017) assuming a central ionizing source and a plane-parallel geometry. Grid 1 is described in Pérez-Montero, 2014 and is calculated using POPSTAR (Mollá et al., 2009) cluster model atmospheres with an instantaneous burst at an age of 1 Myr, assuming a Chabrier, 2003 initial mass function (IMF) and a constant electron density of  $100 \text{ cm}^{-3}$ . Grid 2 is described in Pérez-Montero et al., 2021 and was calculated with cluster model atmospheres from BPASS v.2.1 (Eldridge et al., 2017), assuming an instantaneous burst at an age of 1 Myr, an IMF with slope  $x = -1.35$ , an upper mass limit of  $300 M_{\odot}$ , and binaries. The gas in these models has an electron density of  $100 \text{ cm}^{-3}$ . This grid is recommended for Extreme Emission Line Galaxies (EELGs).

Option 3 can be used to derive chemical abundances in the Narrow Line Regions (NLR) of AGN and includes several grids described in Pérez-Montero et al., 2019a. These assume a double-peaked power law spectral energy distribution with a parameter  $\alpha_{UV} = -1.0$ . The assumed electron density is  $500 \text{ cm}^{-3}$ . The code will ask for the value of  $\alpha_{OX}$  (-0.8 or -1.2) and the criterion used to stop the models (at an outer radius when the fraction of free electrons is 98% or 2%).

All default grids cover an input O/H value in the range [6.9, 9.1] in bins of 0.1 dex and N/O in the range [-2.0, 0.0] in bins of 0.125 dex. Log  $U$  is covered with a resolution of 0.25 dex in the range [-4.0, -1.5] for grids for star-forming regions (i.e., 1 and 2) and in the range [-2.5, -0.5] for grids for AGN. The user can also use their model libraries by including them as a text file in the correct format in the folder `Libraries_opt`. If a different library is introduced by the user (4), the code will automatically check if the file has the correct format. If some information is missing, the code will warn the user about the missing columns.

Once the grid of models has been selected, the code will ask whether to use interpolation between the models in the grid:

Choose models [0] No interpolation [1] Interpolation:

In the interpolated mode, the code makes a linear interpolation of all variables, increasing the resolution by a factor of 10. This prevents the results from clustering around certain grid points. However, this mode slows the calculation time.

As a final step, the program will ask for the constraint laws to limit the grids. This is necessary when a limited set of emission lines is provided and the models must make assumptions about the relations between O/H and N/O (when N/O cannot be derived) or O/H and  $U$  (when no auroral line is provided, so excitation is used to estimate metallicity). For AGNs, there is a degeneracy of the O2O3 emission-line ratio, as discussed in Pérez-Montero et al., 2019a. To derive  $\log U$ , the code will also ask for the preferred  $\log U$  range for the calculations between high-ionization ( $\log U \geq -2.5$ ) or low-ionization ( $\log U \leq -2.5$ ).

Select a file with the constraint laws to limit the grid of models when the measurement of a quantity is impossible without any relation.

#### Default constraints

- (1) Constraints for Star-Forming Galaxies
- (2) Constraints for Extreme Emission Line Galaxies
- (3) Constraints for AGNs (no restriction on the ionization parameter)
- (4) Constraints for high-ionization AGNs ( $\log(U) > -2.5$ )
- (5) Constraints for low-ionization AGNs ( $\log(U) < -2.5$ )

#### Other constraints

- (6) Different constraint file

The user can also use their own constraint assumptions in a text file with the correct format in the folder **Constraints**. If option 6 is chosen, the code will check the file for the correct format. If some information is missing, the code will warn the user about the missing columns.

After this process, the program will summarize the different grids that will be used and the number of models for each grid. From version 5.4 onwards, this process can be sped up by changing the variable **interactive** from **True** to **False** in the script and editing the model parameters and constraints directly in the code.

### 2.4. Results

The code will display the results of the calculations for each row on the screen, along with the task's completeness ratio. At the end, it will generate another **ascii** file containing all the results, named the same as the input file but with the suffix **\_hcm-output.dat**. The first column lists the identification of each row. If this was not specified in the input file, a number will be assigned. The next columns of this file contain the emission-line fluxes used as input, with their corresponding errors.

The next column is an index that indicates whether the whole grid of models has been used or if a constrained grid has been used instead. This depends mainly on the introduced emission lines for each row, as a limited observational set implies additional assumptions to calculate ionic abundances. However, as described above, these constraints can be chosen based on the models, or the user can use their own. An index of 1 indicates that the whole grid of models has been used. This is done when an estimation of the electron temperature, similar to the direct method (see for instance Pérez-Montero, 2017), can be made because both auroral and nebular emission lines are present (e.g.,  $[[\text{O III}]]$  4363

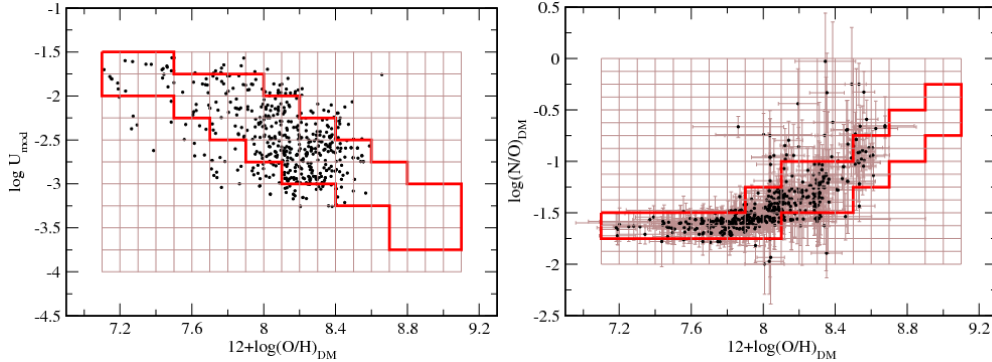


FIGURE 1. Left: relation between total oxygen abundance and ionization parameter for the sample studied in Pérez-Montero, 2014. The solid red line encompasses the most probable combination of parameters occupied by the objects. Right: empirical relation between  $12+\log(\text{O}/\text{H})$  and  $\log(\text{N}/\text{O})$  with the region occupied by the grid of models in the absence of observational information to constrain  $\text{N}/\text{O}$ .

Å with 4959, 5007 Å,  $[[\text{N II}]]$  5755 Å with 6584 Å,  $[[\text{O II}]]$  7325 Å with 3727 Å, or  $[[\text{S III}]]$  6312 Å with 9069, 9532 Å). If any auroral line is not given, which is common in faint or metal-rich nebulae (Pérez-Montero and Díaz, 2005), additional assumptions should be made.

Index 2 represents the case when the electron temperature cannot be estimated, and the code assumes an empirical law between  $\text{O}/\text{H}$  and  $\log U$  (see Figure 1). This relation assumes that metal-poor objects generally exhibit higher excitation, while metal-rich objects have lower excitation. This is the same assumption behind the use of many high- to low-excitation emission line flux ratios (e.g.,  $\text{O3O2}$ ,  $\text{O3N2}$ ) to derive chemical abundances. Finally, index 3 denotes the use of a grid constrained by assuming an empirical relation between  $\text{O}/\text{H}$  and  $\text{N}/\text{O}$ , as shown in Figure 1. This is necessary when  $\text{N}/\text{O}$  cannot be calculated independently in a first iteration using emission-line ratios such as  $\text{N2O2}$ ,  $\text{O3N2}$ , or  $\text{N2S2}$ . This assumption is behind all strong-line calibrations based on  $[[\text{N II}]]$  and implies a constant  $\text{N}/\text{O}$  value for low metallicities due to primarily primary production of  $\text{N}$ , and an increasing  $\text{N}/\text{O}$  with  $\text{O}/\text{H}$  when secondary production of  $\text{N}$  is assumed. This assumption can lead to non-negligible deviations from the real  $\text{O}/\text{H}$  if  $\text{N}/\text{O}$  does not lie in the expected regime, as discussed in Pérez-Montero and Contini, 2009.

The final six columns of the output file give the results for  $\text{O}/\text{H}$ ,  $\text{N}/\text{O}$ , and  $\log U$  with their corresponding errors. If no solution is found,  $\text{O}/\text{H}$  and  $\log U$  are denoted by 0, and  $\text{N}/\text{O}$  is denoted by -10. If the code encounters an error for a specific row of the input, '9999' will be inserted in the output. In this case, the user should review the input lines or contact us for possible inconsistencies.

The results and consistency of the abundances derived from HCM for star-forming objects, whose abundances were derived from the direct method (Pérez-Montero, 2014), and for NLR in AGN as derived using detailed photoionization models (Pérez-Montero et al., 2019a), are well discussed. Nevertheless, in Table 1, I provide a list of the mean offsets and the standard deviation of the residuals of the resulting  $\text{O}/\text{H}$ ,  $\text{N}/\text{O}$ , and  $\log U$  as compared with the input values from the models as a function of the used emission lines. These values illustrate how the code can recover the abundances from the values using only the emission lines as input, but cannot be taken as true uncertainties.

TABLE 1. Mean offsets and standard deviation of the residuals of the resulting properties derived by HCM when the model from POPSTAR emission lines are used as input as a function of the used emission-line ratios.  $[[\text{O III}]]_a$  stands for the  $[[\text{O III}]]$  auroral line at  $\lambda$  4363 Å and  $[[\text{O III}]]_n$  for the nebular lines at  $\lambda$  4959, 5007 Å.

Used lines	Grid	O/H		N/O		log $U$	
		Mean $\Delta$	$\sigma$ res.	Mean $\Delta$	$\sigma$ res.	Mean $\Delta$	$\sigma$ res.
All lines	1	+0.03	0.09	-0.07	0.08	+0.06	0.15
$[[\text{O III}]]_a, [[\text{O III}]]_n, [[\text{N II}]], [[\text{S II}]]$	1	+0.02	0.09	-0.01	0.07	+0.06	0.15
$[[\text{O II}]], [[\text{O III}]]_n, [[\text{N II}]], [[\text{S II}]]$	2	-0.04	0.08	+0.00	0.03	+0.05	0.10
$[[\text{O III}]]_n, [[\text{N II}]], [[\text{S II}]]$	2	-0.03	0.07	+0.00	0.04	+0.05	0.10
$[[\text{O II}]], [[\text{O III}]]_n, [[\text{N II}]]$	2	-0.04	0.24	+0.00	0.23	+0.03	0.09
$[[\text{N II}]], [[\text{S II}]]$	2	+0.00	0.19	+0.00	0.04	+0.02	0.20
$[[\text{O III}]]_n, [[\text{N II}]]$	3	-0.04	0.08	—	—	+0.07	0.13
$[[\text{N II}]]$	3	+0.01	0.15	—	—	+0.03	0.21
$[[\text{O II}]], [[\text{O III}]]_n$	3	+0.00	0.01	—	—	+0.00	0.02
$[[\text{O II}]], [[\text{Ne III}]]$	3	-0.01	0.02	—	—	-0.01	0.03

### 3. HCM in the ultraviolet

The HII-CHI-MISTRY-UV code (hereafter HCM-UV) is similar to the optical version but uses a different set of emission lines in the ultraviolet regime and estimates C/O instead of N/O in the first iteration. It also allows the inclusion of two emission lines in the optical to provide an estimate of the abundance based on an emission-line ratio sensitive to the electron temperature (e.g.,  $[[\text{O III}]] \lambda 5007 / \lambda 1665$ ), although this may introduce larger inaccuracies due to reddening uncertainties. This code is described in Pérez-Montero and Amorín, 2017 for star-forming objects and in Pérez-Montero et al., 2023a for the NLR in AGN.

#### 3.1. Running the Program and Preparing the Input File

Similar to the optical version, it can be executed from the terminal prompt with Python, allowing either calling the script directly or specifying the input file name and the number of iterations for the Monte Carlo simulations:

```
> python HCM-UV_v5.0.py input.txt 100
```

The input file is an `ascii` file whose first row must contain the labels of the used columns, including:

- ID: Identification name for each row.
- `Lya_1216` and `eLya_1216`:  $\text{Ly}\alpha \lambda 1216$  Å and its error.
- `NV_1239` and `eNV_1239`:  $\text{N v} \lambda 1239$  Å and its error.
- `CIV_1549` and `eCIV_1549`:  $\text{C IV} \lambda 1549$  Å and its error.
- `HeII_1640` and `eHeII_1640`:  $\text{He II} \lambda 1640$  Å and its error.
- `OIII_1665` and `eOIII_1665`:  $[\text{O III}] \lambda 1665$  Å and its error. This includes all lines of the  $[\text{O III}]$  multiplet between 1660 Å and 1666 Å.
- `CIII_1909` and `eCIII_1909`:  $\text{C III} \lambda 1909$  Å and its error. Again, this includes all lines of the  $\text{C III}$  multiplet.
- `Hb_4861` and `eHb_4861`:  $\text{H}\beta \lambda 4861$  Å and its error.
- `OIII_5007` and `eOIII_5007`:  $[[\text{O III}]] \lambda 5007$  Å and its error.

The following rows must contain the names and extinction-corrected fluxes in arbitrary

units. A value of zero can be used for missing values, and not all columns are mandatory to get an estimation for O/H, C/O, or  $U$ .

If the input file is correct, the code will prompt for the grid of models and the use of interpolation. For version 5.0, models from POPSTAR, BPASS, and double composite AGN are available. For AGN, the code will ask for the assumed  $\alpha_{OX}$  (-0.8 or -1.2), the stopping criterion for the models (2% or 98).

In the next step, the code will also ask for interpolation of the models to enhance resolution and the choice of templates considering assumptions on the relation between O/H,  $\log U$ , and C/O in case some input emission lines are missing. These templates can be edited by the user in the appropriate folder. As in the optical version, interactivity can be turned off by changing the variable `interactive` from `True` to `False`.

### 3.2. Output File and Analysis of the Results

Once the grid of models is selected, the code will display the results for each input row on the screen, along with the completeness ratio. At the end, it will create an output file in `ascii` format with the results, including all information used for the calculations. The first column is the corresponding ID, and the next columns will be the input emission lines along with their errors.

The next column is an index that indicates if the complete grid has been used (index 1), which occurs only when both  $[[O\ III]]\ \lambda\ 1665$  and  $5007\ \text{\AA}$  are provided to estimate the electron temperature. Index 2 denotes a grid with an implicit relation between O/H and  $\log U$  as shown in Figure 1. Finally, index 3 denotes a grid constrained by assuming a relation between C/O and O/H, similar to that shown in Figure 1 for N/O and O/H, considering a fixed C/N to the solar ratio. This is used when C/O cannot be calculated by means of the emission line ratio C3O3, depending on  $C\ III\ 1909\ \text{\AA}$  and  $[O\ III]\ \lambda\ 1665\ \text{\AA}$ , but an estimate for both O/H and  $\log U$  can be given using C lines. In any case, as commented above, this relation can be changed by the user in the folder `Libraries.uv`. The code, for instance, also provides the relation derived for EELGs given by Pérez-Montero et al., 2021.

The final six columns give the results for O/H, C/O, and  $\log U$  with their corresponding errors. As in the case of the optical version, if no solution can be found for both O/H and  $\log U$ , these are denoted as 0 in the file, and -10 for C/O. A value of 9999 is included when an error for a specific row has been found.

In Table 2 I list the mean offsets and the standard deviation of the residuals when we use as input for the code the same predictions from the models of the grid, when POPSTAR models are used as a function of the different combination of emission lines that lead to a solution. A similar table for the results for AGN can be found in Pérez-Montero et al (2023).

## 4. HCM in the infrared

The program HII-CHI-MISTRY-IR (hereafter HCM-IR) calculates total oxygen abundance, nitrogen-to-oxygen abundance ratio, and the ionization parameter from a set of observed emission lines in the mid-infrared. From version 3.1, the program also supplies a solution for the sulfur abundances. It is described in Fernández-Ontiveros et al., 2021. From version 3.0, the program also admits calculations for the NLR in AGNs, as described in Pérez-Díaz et al., 2022.



TABLE 2. Mean offsets and standard deviation of the residuals of the resulting properties derived by HCM-UV when the model from POPSTAR emission lines are used as input as a function of the used emission-line ratios.

Used lines	Grid	O/H		C/O		log $U$	
		Mean $\Delta$	$\sigma$ res.	Mean $\Delta$	$\sigma$ res.	Mean $\Delta$	$\sigma$ res.
All lines	1	+0.02	0.28	-0.05	0.08	+0.04	0.25
Ly $\alpha$ , C IV], He II, [O III]], C III]	2	+0.02	0.27	-0.06	0.19	+0.05	0.10
C IV], He II, [O III]], C III]	2	+0.10	0.30	-0.14	0.13	-0.11	0.20
Ly $\alpha$ , C IV], He II, C III]	3	+0.00	0.02	–	–	+0.00	0.01
C IV], He II, C III]	3	-0.01	0.03	–	–	+0.00	0.02

#### 4.1. Running the Program and Preparing the Input File

Similarly to the other versions of the program, HCM-IR is executed from a terminal prompt using Python, and the input text file can be invoked in the same command, along with the number of iterations for the Monte Carlo simulations:

```
> python HCM-IR_v3.1.py input.txt 50
```

The input file must be in `ascii` format. The first row specifies the identification of each row and the input emission lines, with the following accepted labels:

- ID: Identification name for each row.
- HI\_4m and eHI\_4m: Pa $\alpha$  at  $\lambda$  4.07  $\mu\text{m}$  and its error.
- ArII\_7m and eArII\_7m: [[Ar III]] at  $\lambda$  6.98  $\mu\text{m}$  and its error.
- HI\_7m and eHI\_7m: Br $\alpha$  at  $\lambda$  7.46  $\mu\text{m}$  and its error.
- ArV\_8m and eArV\_8m: [[Ar IV]] at  $\lambda$  7.90  $\mu\text{m}$  and its error.
- ArIII\_9m and eArIII\_9m: [[Ar III]] at  $\lambda$  8.99  $\mu\text{m}$  and its error.
- SIV\_10m and eSIV\_10m: [[S IV]] at  $\lambda$  10.5  $\mu\text{m}$  and its error.
- HI\_12m and eHI\_12m: Hu $\alpha$  at  $\lambda$  12.46  $\mu\text{m}$  and its error.
- NeII\_12m and eNeII\_12m: [[Ne II]] at  $\lambda$  12.8  $\mu\text{m}$  and its error.
- ArV\_13m and eArV\_13m: [[Ar V]] at  $\lambda$  13.1  $\mu\text{m}$  and its error.
- NeV\_14m and eNeV\_14m: [Ne V] at  $\lambda$  14.9  $\mu\text{m}$  and its error.
- NeIII\_15m and eNeIII\_15m: [[Ne III]] at  $\lambda$  15.5  $\mu\text{m}$  and its error.
- SIII\_18m and eSIII\_18m: [[S III]] at  $\lambda$  18.8  $\mu\text{m}$  and its error.
- NeV\_24m and eNeV\_24m: [Ne V] at  $\lambda$  24.3  $\mu\text{m}$  and its error.
- OIV\_25m and eOIV\_25m: [O IV] at  $\lambda$  25.9  $\mu\text{m}$  and its error.
- SIII\_33m and eSIII\_33m: [[S III]] at  $\lambda$  33.7  $\mu\text{m}$  and its error.
- OIII\_52m and eOIII\_52m: [[O III]] at  $\lambda$  52  $\mu\text{m}$  and its error.
- NII\_57m and eNII\_57m: [[N II]] at  $\lambda$  57  $\mu\text{m}$  and its error.
- OIII\_88m and eOIII\_88m: [[O III]] at  $\lambda$  88  $\mu\text{m}$  and its error.
- NII\_122m and eNII\_122m: [[N II]] at  $\lambda$  122  $\mu\text{m}$  and its error.
- NII\_205m and eNII\_205m: [[N II]] at  $\lambda$  205  $\mu\text{m}$  and its error.

Then the program will ask for the chosen grid of models. For version 3.0, models from POPSTAR, BPASS, and double composite AGN are available. In the case of AGN, the code will ask for the assumed  $\alpha_{OX}$  (-0.8 or -1.2), and the stopping criterion for the models (2% or 98% of free electrons). In addition, as in other versions, it is possible to incorporate other grids defined by the user, conveniently specified and stored in the `Libraries_ir` folder. The code will also ask about the possibility of model interpolation to increase by a factor of 10 the resolution of the grid, but this can slow down the calculation

TABLE 3. Mean offsets and standard deviation of the residuals of the resulting properties derived by HCM-IR when the models from POPSTAR emission lines are used as input as a function of the used emission-line ratios.

Used lines	Grid	O/H		N/O		log $U$	
		Mean $\Delta$	$\sigma$ res.	Mean $\Delta$	$\sigma$ res.	Mean $\Delta$	$\sigma$ res.
All lines	2	+0.04	0.09	-0.00	0.01	+0.02	0.07
[[Ne II]], [[Ne III]], [[S II]], [[S IV]], [[O III]], [[N II]], [[N III]]	2	+0.03	0.13	+0.00	0.01	+0.02	0.07
[[O III]], [[N II]], [[N III]]	2	-0.01	0.18	+0.00	0.01	+0.02	0.15
<i>HI</i> , [[S III]], [[S IV]], [[Ne II]], [[Ne III]]	3	+0.04	0.04	—	—	-0.01	0.01
[[S III]], [[S IV]], [[Ne II]], [[Ne III]]	3	+0.04	0.04	—	—	+0.00	0.01
[[S III]], [[S IV]]	3	+0.02	0.02	—	—	+0.00	0.01
[[Ne II]], [[Ne III]]	3	+0.03	0.09	—	—	+0.00	0.06
[[N II]], [[N III]]	3	+0.00	0.11	—	—	+0.00	0.06

time. Finally, the code will ask for constraints to consider when not all emission lines can be used. Again, the code can provide templates calculated for star-forming galaxies by Pérez-Montero, 2014, for EELGs by Pérez-Montero et al., 2021, or assuming low- or high-excitation AGNs. In any case, other constraint files can be incorporated by the user, and the level of interaction at the beginning of the code can be reduced by editing the variable `interactive` directly in the script.

#### 4.2. Output File and Analysis of the Results

As in previous versions of HCM, once the grid of models has been selected, the code will display results for O/H, N/O

### 5. HCM for the Calculation of $T_*$

The HII-CHI-MISTRY-TEFF (hereafter HCM-TEFF) is different from the previously described versions of HCM, as its aim is not the derivation of chemical abundances, but the calculation of the equivalent effective temperature of the ionizing source ( $T_*$  or  $T_{eff}$ ) or the fraction of absorbed ionizing photons assuming a matter-bounded geometry ( $f_{abs}$ ). This code makes use of the relation between the so-called softness parameter (Vilchez and Pagel, 1988, Pérez-Montero and Vilchez, 2009) and the hardness of the ionizing incident radiation, and the program is well described in Pérez-Montero et al., 2019b and Pérez-Montero et al., 2020. In addition, a discussion on the effect of the diffuse ionized gas (DIG) on the results when using certain low-excitation lines, such as [[S II]], is also discussed in Pérez-Montero et al., 2023b. An independent version for the infrared, only valid so far for the derivation of  $T_*$  and  $U$ , is also available and described in Pérez-Montero et al., 2024..

#### 5.1. Running the Program and Preparing the Input File

Running the program is equivalent to the previous versions of HCM, through the terminal prompt:

```
> HCM-Teff_v5.2.py input.txt 50
```

The input file must be written in `ascii` format. The first row should correspond to

the object ID and the labels of the used emission lines and, if available, the oxygen abundance, which can reduce the uncertainty. The code accepts the following labels:

- ID: Identification name for each row.
- 12logOH and e12logOH: Total oxygen abundance  $12+\log(\text{O}/\text{H})$  and its error. This may be calculated using HCM in a previous iteration.
- CIV\_1549 and eCIV\_1549:  $\text{C IV } \lambda 1549 \text{ \AA}$  and its error.
- CIII\_1909 and eCIII\_1909:  $\text{C III } \lambda 1909 \text{ \AA}$  and its error. This should include all lines taking part in the multiplet around this wavelength.
- OII\_3727 and eOII\_3727:  $[\text{O II}] \lambda 3727 \text{ \AA}$  and its error. As in the case of HCM, this represents the addition of the two lines of the doublet of  $[\text{O II}]$  if there is good spectral resolution.
- OIII\_4959 and eOIII\_4959:  $[\text{O III}] \lambda 4959 \text{ \AA}$  and its error.
- OIII\_5007 and eOIII\_5007:  $[\text{O III}] \lambda 5007 \text{ \AA}$  and its error. As in the case of HCM, if only one of the two lines of the  $[\text{O III}]$  doublet (4959, 5007) is introduced, the code assumes its addition taking into account its theoretical relation.
- HeI\_4471 and eHeI\_4471:  $\text{He I } \lambda 4471 \text{ \AA}$  and its error.
- HeI\_5876 and eHeI\_5876:  $\text{He I } \lambda 5876 \text{ \AA}$  and its error.
- HeI\_6678 and eHeI\_6678:  $\text{He I } \lambda 6678 \text{ \AA}$  and its error.
- HeII\_4686 and eHeII\_4686:  $\text{He II } \lambda 4686 \text{ \AA}$  and its error.
- SII\_6716 and eSII\_6716:  $[\text{S II}] \lambda 6716 \text{ \AA}$  and its error.
- SII\_6731 and eSII\_6731:  $[\text{S II}] \lambda 6731 \text{ \AA}$  and its error. It is also possible to use the addition of the two  $[\text{S II}]$  lines using SII\_6725 and eSII\_6725.
- SIII\_9069 and eSIII\_9069:  $[\text{S III}] \lambda 9069 \text{ \AA}$  and its error.
- SIII\_9532 and eSIII\_9532:  $[\text{S III}] \lambda 9532 \text{ \AA}$  and its error. As in the case of  $[\text{O III}]$ , if one of the two  $[\text{S III}]$  nebular lines is not introduced, the code assumes its addition taking the theoretical expected ratio.
- ArIV\_4740 and eArIV\_4740:  $[\text{Ar IV}] \lambda 4740 \text{ \AA}$  and its error.
- ArIII\_7135 and eArIII\_7135:  $[\text{Ar III}] \lambda 7135 \text{ \AA}$  and its error.
- NII\_6584 and eNII\_6584:  $[\text{N II}] \lambda 6584 \text{ \AA}$  and its error.

The next rows in the input file should correspond to the different values for which the code should derive  $T_*$  and  $\log U$ . The provided emission line fluxes must be reddening corrected, but it is not necessary that they are relative to  $\text{H}\beta$ , as only ratios of lines of different ionization are used. Use 0 when no value is found for a line or error.

## 5.2. The Grids of Models

If the input file is correct and the variable `interactive` is set to `True` in the code, it will ask for the parameters we want to calculate:

- (1) Effective temperature and ionization parameter
- (2) Photon absorption fraction and ionization parameter

Choose derived parameters:

Depending on these parameters, the code will ask for different grids of models and geometries. In the case of  $T_{eff}$ :

- (1) WM-Basic (30–60 kK)
- (2) WM-Basic (30–60 kK) and Rauch (80–120 kK) stellar atmospheres
- (3) Black body (30–100 kK)

Choose models:

Option 1 calculates  $T_*$  and  $\log U$  using WM-BASIC single star atmospheres from Pauldrach et al., 2001 from 30 to 60 kK, while option 2 extends the range up to 120 kK using post-AGB stellar atmospheres from Rauch. Option 3 uses black-body spectral energy distributions in the range 30-100 kK.

It is known that the geometry assumed in the models can affect their position on the softness diagrams, so the code will also ask for this in this case:

- (1) Plane-parallel geometry
- (2) Spherical geometry

Choose geometry of the models:

If we want to calculate the photon absorption factor,  $f_{abs}$ , defined as the ratio of ionizing hydrogen photons that do not escape from the nebula, along with  $\log U$ , this is calculated using cluster model atmospheres from BPASS v.2.1 from Eldridge et al., 2017, assuming an instantaneous burst at 4 Myr, with binaries and an IMF with slope  $X = -1.35$  and an upper mass limit of  $300 M_\odot$ . In this case, we can choose among models with stellar metallicity identical to that of the gas in each model, or either assume nearly metal-free stars ( $Z = 10^{-5}$ ). The code also supplies models with black-body with  $T_* = 10^5$  K, equivalent for metal-free stars.

- (1) BPASS cluster atmospheres, age = 4 Myr,  $M_{up} = 300$ ,  $x = 1.35$ , w/binaries,  $Z_* = Z_g$
- (2) BPASS cluster atmospheres, age = 4 Myr,  $M_{up} = 300$ ,  $x = 1.35$ , w/binaries,  $Z_* = 1e-5$
- (3) Black-body,  $T_* = 1e5$  K

In this case, only spherical geometry models are considered.

In Figure 2, two examples of the behavior of the grids of models in one of the softness diagrams are shown, as in Pérez-Montero et al., 2020, illustrating how the grids of models cover the space of the emission line ratios.

Finally, the code will ask for the possibility of using interpolation in the final chosen grid:

Choose

### 5.3. Output file and analysis of the results

As in other versions of HCM, the code will show on the screen the results for each row of the input file along with the ratio of completeness of the task. At the end it will create an output file called as the name of the input file adding `_hcm-teff--ouput.dat`. This file contains all the information for the assumed grids and the results for each one of the rows.

The first column corresponds to the identification of each row while the next ones correspond to the input fluxes of the emission lines. The next two correspond to the assumed O/H, with 0 if no value was introduced. Finally, the four last columns correspond to the calculated  $T_*$  (or  $f_{abs}$  if the grid 3 was chosen) and  $\log U$  with their errors. A value 0 is assigned if no solution is found or the introduced lines are not enough. A value -99999 will be introduced in case the code finds any error for a specific input row.

In Table 4 I list the mean offsets and the standard deviation of the residuals

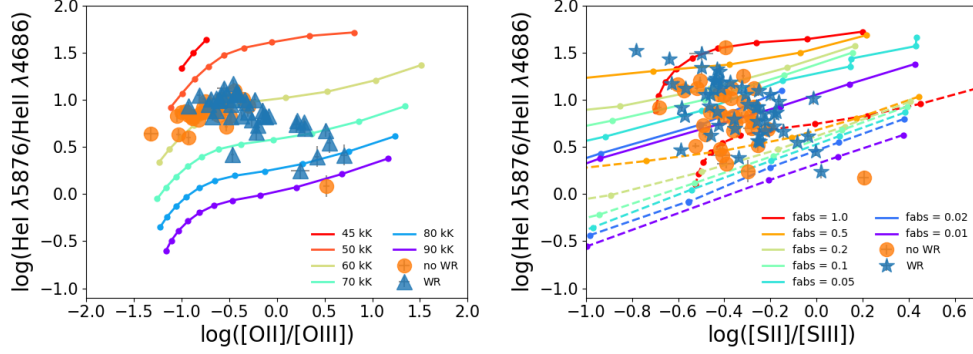


FIGURE 2. Examples of two softness diagrams for the sample of He II-emitters presented in Pérez-Montero et al., 2020. At left  $[[\text{O II}]]/[[\text{O III}]]$  vs  $\text{He I}/\text{He II}$  with models at  $12+\log(\text{O}/\text{H})$  and different values for  $T_*$  and, at right, using  $[[\text{S II}]]/[[\text{S III}]]$  and BPASS models assuming different values for  $f_{abs}$ . In all sequences values in the lower left part correspond to higher values for  $\log U$ .

TABLE 4. Mean offsets and standard deviation of the residuals of the resulting properties derived by HCM-TEFF when the model emission lines are used as input as a function of the used emission-line ratios.

Used line ratios	$T_*$ (kK) <sup>†</sup>		$\log U^a$		$\log f_{abs}^\ddagger$		$\log U^b$	
	Mean $\Delta$	$\sigma$ res.	Mean $\Delta$	$\sigma$ res.	Mean $\Delta$	$\sigma$ res.	Mean $\Delta$	$\sigma$ res.
$[[\text{O II}]]/[[\text{O III}]]$ , $[[\text{S II}]]/[[\text{S III}]]$ , $\text{He I}/\text{He II}$	+0.8	2.1	+0.01	0.10	+0.11	0.34	-0.10	0.53
$[[\text{O II}]]/[[\text{O III}]]$ , $\text{He I}/\text{He II}$	+0.8	2.1	+0.01	0.10	-0.12	0.27	+0.14	0.47
$[[\text{S II}]]/[[\text{S III}]]$ , $\text{He I}/\text{He II}$	+0.6	2.0	+0.03	0.13	-0.19	0.35	+0.10	0.62
$[[\text{S II}]]/[[\text{O III}]]$ , $\text{He I}/\text{He II}$	-0.3	5.1	+0.04	0.51	-0.07	0.27	-0.10	0.59
$\text{He I}/\text{He II}$	-0.5	6.8	+0.04	0.72	-0.12	0.35	-0.25	0.63

for the obtained final results as a function of the input emission lines when compared with the input information from the code.

#### 5.4. The HCM-TEFF-IR version

A similar code is available for its use based only on mid-IR emission-lines. Although it is planned to merge it with the optical version, so far it works in an independent module. It is described and applied in Pérez-Montero et al., 2024 to calculate  $T_*$  for star-forming regions and in Pérez-Montero et al. (submitted) to calculate  $\alpha_{OX}$  in AGN, taking advantage of the high-excitation lines that can be measured in this regime.

It basically works in the same way as it is described above, using exactly the same grids of models with the exception of those calculated for the derivation of the photon absorption factor. New models have been also calculated for AGN in order to cover a wide range for  $\alpha_{OX}$  in the range  $[-2.0, -1.0]$  and  $\log U$  in the range  $[-4.0, -1.0]$  for oxygen abundances from  $12+\log(\text{O}/\text{H})$  from 8.1 to 9.0. The user can select for this modality between models with or without dust grains mixed in the gas and test different stopping criteria in the models

(2%, 98%, and 99.9% of free electrons) what gives the possibility of exploring the weight in the results of the low-excitation zone in the integrated spectrum.

The instructions and steps are the same, but using in the input the following emission-lines, in addition to the ID and metallicity entries:

- ArIII\_7m and ArIII\_7m for [[Ar III]] at  $\lambda$  6.98  $\mu\text{m}$  and its error.
- ArIV\_8m and ArIV\_8m for [[Ar IV]] at  $\lambda$  7.90  $\mu\text{m}$  and its error.
- ArIII\_9m and ArIII\_9m for [[Ar III]] at  $\lambda$  8.99  $\mu\text{m}$  and its error.
- SIV\_10m and eSIV\_10m for [[S IV]] at  $\lambda$  at 10.5  $\mu\text{m}$  and its error.
- NeII\_12m and eNeII\_12m for [[Ne II]]  $\lambda$  12.8  $\mu\text{m}$  and its error.
- ArV\_13m and ArV\_13m for [[Ar V]] at  $\lambda$  13.1  $\mu\text{m}$  and its error.
- NeV\_14m and eNeV\_14m for [NeV]  $\lambda$  14.9  $\mu\text{m}$  and its error.
- NeIII\_15m and eNeIII\_15m for [[Ne III]]  $\lambda$  15.5  $\mu\text{m}$  and its error.
- SIII\_18m and eSIII\_18m for [[S III]]  $\lambda$  18.8  $\mu\text{m}$  and its error.
- NeV\_24m and eNeV\_24m for [NeV]  $\lambda$  24.3  $\mu\text{m}$  and its error.
- OIV\_25m and eOIV\_25m for [O IV]  $\lambda$  25.9  $\mu\text{m}$  and its error.
- SIII\_33m and eSIII\_33m for [[S III]]  $\lambda$  at 33.7  $\mu\text{m}$  and its error.
- OIII\_52m and OIII\_52m for [[O III]]  $\lambda$  52  $\mu\text{m}$  and its error.
- NII\_57m and eNII\_57m for [[N II]]  $\lambda$  57  $\mu\text{m}$  and its error
- OIII\_88m and eOIII\_88m for [[O III]]  $\lambda$  88  $\mu\text{m}$  and its error
- NII\_122m and eNII\_122m for [[N II]]  $\lambda$  122  $\mu\text{m}$  and its error.
- NII\_205m and eNII\_205m for [[N II]]  $\lambda$  205  $\mu\text{m}$  and its error.

In this case, the code uses as observables ratios of low- to -high-ionization IR emission-lines that can also be used to construct the corresponding IR softness diagram (e.g. [[Ne II]]/[[Ne III]], [[S III]]/[[S IV]]). As compared to the optical version, this version is less affected by DIG contribution as it involves higher excitation emission-lines.

The very high excitation lines, such as [[O IV]] or [[Ne V]] can also be used to discriminate very hard incident SEDs. In the case of AGN the line ratios can only be used to provide an estimate of the hardness when they involve very high-excitation lines (e.g. ([[Ne II]]+[[Ne III]])/[[Ne V]] or [[O III]]/[[O IV]], or ([[S III]]+[[S IV]])/[[O IV]]).

## Acknowledgements

All versions and articles of the project HII-CHI-MISTRY have been possible to the financial support from the different editions of the Coordinated project of the Spanish Plan Nacional de astronomía y Astrofísica Estallidos de Formación Estelar en Galaxias: Estallidos 5, Estallidos 6, Estallidos 7, and Estallidos 8.

## REFERENCES

- Chabrier, G. (2003). The Galactic Disk Mass Function: Reconciliation of the Hubble Space Telescope and Nearby Determinations. *ApJ*, 586:L133–L136.
- Eldridge, J. J., Stanway, E. R., Xiao, L., McClelland, L. A. S., Taylor, G., Ng, M., Greis, S. M. L., and Bray, J. C. (2017). Binary Population and Spectral Synthesis Version 2.1: Construction, Observational Verification, and New Results. *PASA*, 34:e058.
- Ferland, G. J., Chatzikos, M., Guzmán, F., Lykins, M. L., van Hoof, P. A. M., Williams, R. J. R., Abel, N. P., Badnell, N. R., Keenan, F. P., Porter, R. L., and Stancil, P. C. (2017). The 2017 Release Cloudy. *RMxAA*, 53:385–438.
- Fernández-Ontiveros, J. A., Pérez-Montero, E., Vílchez, J. M., Amorín, R., and Spinoglio, L.

- (2021). Measuring chemical abundances with infrared nebular lines: HII-CHI-MISTRY-IR. *A&A*, 652:A23.
- Mollá, M., García-Vargas, M. L., and Bressan, A. (2009). PopStar I: evolutionary synthesis model description. *MNRAS*, 398:451–470.
- Pauldrach, A. W. A., Hoffmann, T. L., and Lennon, M. (2001). Radiation-driven winds of hot luminous stars. XIII. A description of NLTE line blocking and blanketing towards realistic models for expanding atmospheres. *A&A*, 375:161–195.
- Pérez-Díaz, B., Pérez-Montero, E., Fernández-Ontiveros, J. A., and Vílchez, J. M. (2022). Measuring chemical abundances in AGN from infrared nebular lines: HII-CHI-MISTRY-IR for AGN. *A&A*, 666:A115.
- Pérez-Montero, E. (2014). Deriving model-based  $T_e$ -consistent chemical abundances in ionized gaseous nebulae. *MNRAS*, 441(3):2663–2675.
- Pérez-Montero, E. (2017). Ionized Gaseous Nebulae Abundance Determination from the Direct Method. *PASP*, 129(974):043001.
- Pérez-Montero, E. and Amorín, R. (2017). Using photo-ionisation models to derive carbon and oxygen gas-phase abundances in the rest UV. *MNRAS*, 467(2):1287–1293.
- Pérez-Montero, E., Amorín, R., Pérez-Díaz, B., Vílchez, J. M., and García-Benito, R. (2023a). Assessing model-based carbon and oxygen abundance derivation from ultraviolet emission lines in AGNs. *MNRAS*, 521(1):1556–1569.
- Pérez-Montero, E., Amorín, R., Sánchez Almeida, J., Vílchez, J. M., García-Benito, R., and Kehrig, C. (2021). Extreme emission-line galaxies in SDSS - I. Empirical and model-based calibrations of chemical abundances. *MNRAS*, 504(1):1237–1252.
- Pérez-Montero, E. and Contini, T. (2009). The impact of the nitrogen-to-oxygen ratio on ionized nebula diagnostics based on [NII] emission lines. *MNRAS*, 398:949–960.
- Pérez-Montero, E. and Díaz, A. I. (2005). A comparative analysis of empirical calibrators for nebular metallicity. *MNRAS*, 361(3):1063–1076.
- Pérez-Montero, E., Dors, O. L., Vílchez, J. M., García-Benito, R., Cardaci, M. V., and Hägele, G. F. (2019a). A bayesian-like approach to derive chemical abundances in type-2 active galactic nuclei based on photoionization models. *MNRAS*, 489(2):2652–2668.
- Pérez-Montero, E., Fernández-Ontiveros, J. A., Pérez-Díaz, B., Vílchez, J. M., Kumari, N., and Amorín, R. (2024). Exploring the hardness of the ionising radiation with the infrared softness diagram. I. Similar effective temperature scales for starbursts and (ultra)luminous infrared galaxies. *A&A*, 684:A40.
- Pérez-Montero, E., García-Benito, R., and Vílchez, J. M. (2019b). Revisiting the hardening of the stellar ionizing radiation in galaxy discs. *MNRAS*, 483:3322–3335.
- Pérez-Montero, E., Kehrig, C., Vílchez, J. M., García-Benito, R., Duarte Puertas, S., and Iglesias-Páramo, J. (2020). Photon leaking or very hard ionizing radiation? Unveiling the nature of He II-emitters using the softness diagram. *A&A*, 643:A80.
- Pérez-Montero, E. and Vílchez, J. M. (2009). On the hardening of the ionizing radiation in HII regions across galactic discs through softness parameters. *MNRAS*, 400:1721–1725.
- Pérez-Montero, E., Zinchenko, I. A., Vílchez, J. M., Zurita, A., Florido, E., and Pérez-Díaz, B. (2023b). The softness diagram for MaNGA star-forming regions: diffuse ionized gas contamination or local HOLMES predominance? *A&A*, 669:A88.
- Vílchez, J. M. and Pagel, B. E. J. (1988). On the determination of temperatures of ionizing stars in H II regions. *MNRAS*, 231:257–267.